Journal of Materials Chemistry A

Accepted Manuscript

ROYAL SOCIETY OF CHEMISTRY

www.rsc.org/materialsA

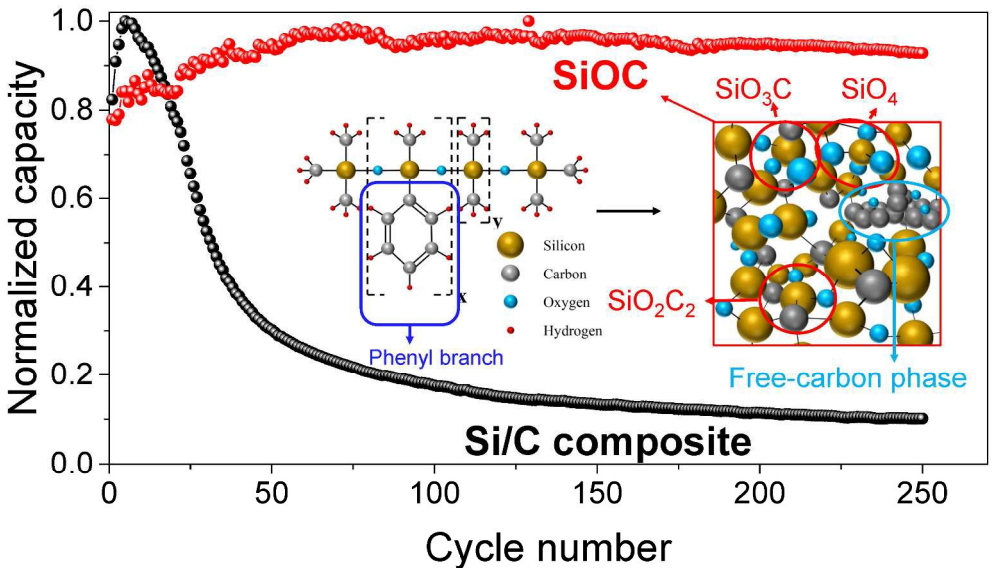

299x175mm (300 x 300 DPI)

Journal of Materials Chemistry A

ARTICLE

Phenyl-Rich Silicone Oil as a Precursor for SiOC Anode Materials in Long-Cycle and High-Rate Lithium Ion Batteries†

Received 00th January 20xx,
Accepted 00th January 20xx

DOI: 10.1039/x0xx00000x

www.rsc.org/

Martin Halim, ‡[a,b] Chairul Hudaya, ‡[a,b,c] A-Young Kim[a,d] and Joong Kee Lee*[a,b]

Silicon oxycarbide (SiOC) is gaining increasing attention as a promising anode material for lithium ion batteries due to its higher reversible capacity compared to incumbent graphite. The kinetic processes at a SiOC anode result in rapid capacity fading even at a relatively low current density, thereby hindering its commercialization. Herein, a distinctive, phenyl-rich silicone oil is used as a precursor for producing SiOC anode materials via simple pyrolysis. We find that only silicone oil with phenyl-rich rings can be converted into SiOC material. The phenyl group was crucial for carbon incorporation to allow Si-O-C bonding and the formation of a free-carbon phase. The resulting SiOC anode exhibited stable cyclability up to 250 cycles, with a discharge capacity of 800 $mAhg^{-1}$ at a current density of 200 mAg^{-1}. The remarkable cycle performance of SiOC was correlated to its low dimensional expansion (7%) during lithiation, which maintains its structure over cycling. Rate capability tests showed a highly stable performance with a maximum discharge capacity of 852 $mAhg^{-1}$ at a current density of 100 mAg^{-1}. When the discharge current density was increased 64-fold, the reversible capacity of the SiOC anode was 90% of its maximum capacity, 772 $mAhg^{-1}$. The excellent electrochemical performance of SiOC could be attributed to the rapid mobility of Li^+ within the SiOC matrix, as indicated by a Li^+ diffusion coefficient of 5.1×10^{-6} cm^2 s^{-1}.

Introduction

Rechargeable lithium ion batteries (LIBs) are of interest due to their high energy density, moderate capability, and long cycle life. These properties are responsible for their widespread applications that range from portable devices to electric vehicles.[1-5] Nevertheless, LIBs largely rely on carbonaceous materials (i.e. graphite) that have a theoretical capacity of 372 $mAhg^{-1}$.[6] Tremendous efforts are devoted towards the replacement of carbonaceous anodes with materials that possess a higher reversible capacity.

Silicon has gained considerable attention due to its high theoretical capacity of 4200 $mAhg^{-1}$ in the fully lithiated state ($Li_{4.4}Si$). The major drawback of Si stems from its inherent properties that result in excessive volume changes of over 300%, leading to significant capacity fading due to cracking and loss of conductivity.[7-9] In contrast, the relatively small volume change of carbonaceous materials (~10%) results in improved cyclability.[10] Hence, numerous attempts for developing a composite material comprising Si and C that harnesses the advantages of its individual elements have been realized. Investigations of Si/C composites revealed that carbon acts as a buffer layer that suppresses large volume changes, thereby maintaining structural stability.[11] However, the issue of capacity fading in conventional Si/C composites remains unresolved since volume expansion-compression and structural breakdown occur extensively.[11]

Silicon oxycarbide (SiOC) comprises a new class of high-capacity anode materials that has the potential to replace carbonaceous and silicon-based anodes. Several studies on SiOC anodes for LIBs have been carried out in succession of the pioneering work of the Dahn group.[12] The reversible capacity of SiOC is ~666 $mAhg^{-1}$, almost two-fold higher than that of graphite.[13] SiOC can be synthesized via pyrolysis of a polymer-derived ceramic precursor (PDC) such as polymethylphenylsiloxane,[12] polyphenylmethylsilane/pitch mixture,[14] polysiloxane,[15] polyhydrodimethylsiloxane (PHMS)/graphene oxide mixture,[16] tetramethyl-tetravinylcyclotetrasiloxane/dicumyl peroxide mixture,[17] polyramic RD-684,[13, 18] and PHMS/platinum divinyltetramethyldisiloxane/divinylbenzene mixture.[19] Alternatively, SiOC can be electrodeposited through reduction of silicon tetrachloride ($SiCl_4$) in a propylene carbonate solution to form a SiOC thin film.[20] The cycle performance of SiOC anodes is still far from practical requirements. To date, the best cycle performance has been reported by Ahn and co-worker, i.e. stability up to 60 cycles and delivered 637 $mAhg^{-1}$ at 100 mAg^{-1}.[17] While Riedel's group performed extensive

[a] Center for Energy Convergence, Korea Institute of Science and Technology, Seoul 02792, Republic of Korea. *E-mail: leejk@kist.re.kr
[b] Energy and Environmental Engineering, Korea University of Science and Technology, Daejeon 34113, Republic of Korea.
[c] Department of Electrical Engineering, Faculty of Engineering, Universitas Indonesia, Depok 16424, Republic of Indonesia.
[d] Department of Material Science and Engineering, Korea University, Seoul 02841, Republic of Korea.

‡ These authors contributed equally to this work

† Electronic Supplementary Information (ESI) available: digital image of as-prepared SiOC, TGA analysis, XPS analysis, rate capability, CV analysis, Li^+ diffusion and electrochemical comparison among SiOC precursors.
See DOI: 10.1039/x0xx00000x

studies on SiOC materials, they focused on rate capability tests using prolonged cycles rather than expounding on the cell cycle performance.[13, 18, 19, 21-23]

In this work, we demonstrate the use of a novel SiOC anode material derived from commercially available silicone oil, which is synthesized using a simple, pyrolysis method. Silicone oil, a member of the polysiloxane group with organic side chains, has a high thermal stability and is therefore used as a lubricant in the aerospace industry.[24] In addition, it is an odourless, non-flammable, non-toxic and environmentally friendly precursor. As-prepared SiOC anodes derived from silicone oil exhibit remarkable electrochemical performance, as represented by high discharge capacity, excellent rate capability and long cyclability.

Experimental

Synthesis of SiOC material

The SiOC powder was produced via pyrolysis of commercial silicone oil precursors. Three different precursors from three suppliers, Bratachem (BRA), AP Resources Co. (APR) and Sigma Aldrich (SIG), were used. BRA and APR have the same chemical formula, dimethylpolysiloxane, while SIG is poly(dimethylsiloxane-*co*-methylphenylsiloxane). Silicone oil precursors were used as received without any treatment. Pyrolysis was conducted in a quartz tube furnace with an Ar gas flow rate of 200 sccm. Samples were heated at a rate of 300 $^{o}Ch^{-1}$ to 900 ^{o}C, maintained at this temperature for 1 h and then left to cool to room temperature (25 ^{o}C).

Characterization of SiOC

The chemical bonding in the silicone oil was confirmed by Fourier transform infrared spectroscopy (FTIR, Thermo, IS 10). The structure of SiOC was confirmed by X-ray Diffraction (XRD, Rigaku, Ultima IV) using monochromatic Cu K_{α} at 40 kV and 100 mA. Thermogravimetric analysis (TGA, SDT Q600 and TA Instruments) at an Ar flow rate of 200 sccm and heating rate of 300 $^{\circ}C\ h^{-1}$ was conducted to determine the silicone oil weight loss profile with increasing temperature. Morphological images of SiOC were captured using scanning electron microscopy (SEM, FEI Company). The free-carbon phase in SiOC was confirmed by Raman spectroscopy (Renishaw, InVia Raman Microscope) in the range of 500–3500 cm^{-1}. The distribution of Si, O and C in the bulk SiOC was mapped using high-resolution transmission electron microscopy (HRTEM, FEI Company, Tecnai G2), while the elemental analysis of SiOC was carried out by energy dispersive X-ray (EDX, FEI Company, Tecnai G2). The chemical composition of SiOC powder was further confirmed by X-ray photoelectron spectroscopy (XPS, Ulvac-PHI, 5000 Versaprobe) performed under an Ar atmosphere with a monochromatic Al K_{α} X-ray source at 117.4 eV, as well as by X-ray fluorescence (XRF, Rigaku ZSZ Primum II, Japan).

Synthesis of Si/C composite

The Si/C composite was prepared by mixing 60 wt.% of pristine Si powder (99%, 5 µm average diameter, SMC, Japan) and 40 wt.% of mesocarbon microbeads (MCMB, Sigma Aldrich). The Si and C powder were combined in a stainless steel vessel (SPEX SamplePrep 8007) consisting of 20 balls, each with 5 mm diameter, and 9 balls each with 9.5 mm diameter. A total ball weight of ~40 g and total powder weight of 2 g were used to achieve a ball to powder (BTP) ratio of 20:1. The powder was then poured into a stainless steel vessel inside a glove box under Ar atmosphere to prevent oxygen contamination, which could trigger oxidation during ball milling. The stainless steel vessel was then placed in a high-energy ball milling machine (8000D Mixer/Mill ®) and rotated for 10 min.

Electrochemical methods

The SiOC anodes were prepared by mixing 60 wt.% of SiOC powder, 20 wt.% of Denka black and 20 wt.% of polyacrylic acid (PAA) in ethanol solution. The slurry was mixed in a mini-mill grinder (Laval Lab) for 30 min. After that, the slurry was cast on copper foil (battery grade) and dried for 8 h. The dried electrode was then cut into circular working electrodes (12 mm in diameter) prior to assembly into coin-type (CR2032) cells. Thin film Li metal, polypropylene and 1 M $LiPF_6$ (PANAX ETEC Co., Ltd) dissolved in EC:DMC:EMC (1:1:1, vol.%) were used as the counter electrode, separator and electrolyte, respectively. The Si/C composite was assembled in a manner similar to the SiOC electrodes. The as-prepared electrodes were then subjected to various electrochemical tests, including galvanostatic, rate capability and cyclic voltammetry (CV) tests. Galvanostatic and rate capability tests were conducted in a Maccor system (series 4000). The CV test was conducted in a multi-channel potentiostat VMP3 (Bio-logic).

Results and discussion

The experiments were initially conducted using three widely available silicone oils in the market: BRA, APR and SIG. Each silicone oil precursor was annealed in a quartz tube furnace under equal treatments. Surprisingly, only SIG resulted in a black-solid material at the bottom of the quartz tube (Fig. S1†), while the other precursors showed an absence of this material. This interesting finding spurred our investigation of the chemical properties of the three silicone oils precursors. Fig. 1 shows the FTIR spectra of the as-received samples prior to annealing in the 650 to 2000 cm^{-1} range. All samples showed three intense bands at 785, 1016 and 1258 cm^{-1}, indicating the R-Si-O(methyl)$_2$, Si-O-Si and R-Si-O(methyl)$_2$ groups, respectively.[25] However, only SIG sample demonstrated extensive Si-phenyl bonding at 694, 730 and 1430 cm^{-1}, representing the R-Si(phenyl)$_2$O-R, R-Si(methyl)(phenyl)O-R and Si-phenyl groups, respectively.[25] Hence, we believe the evolution of the phenyl-rich group on the SIG silicone oil precursor played a key role in producing the black material residue found inside the furnace during pyrolysis.

Our hypothesis was further supported by the TGA analysis (Fig. S2†), which showed that the weight loss of both BRA and APR precursors was >99 %. In contrast, the weight loss of the SIG precursor was ~94 %. Although the TGA analysis showed that the remaining material was ~6 %, our experimental range revealed that about 20 wt.% of the SIG precursor could be converted to SiOC. The phenyl functional group was crucial for facilitating carbon introduction to form Si-O-C bond combinations such as SiO_4, SiO_3C, SiO_2C_2, SiO_3C and SiC.[26, 27] Furthermore, the benzene ligand could suppress the weight reduction due to the carbon loss experienced during pyrolysis, providing a large amount of free-carbon in the ceramic matrix.[28, 29] We performed XRD analysis to reveal the structural properties of the as-prepared SiOC from SIG (inset Fig. 1). No considerable peak was detected from the XRD pattern, indicating the amorphous state of SiOC. This result is in good agreement with other previous works on SiOC materials obtained from different precursors.[30, 31]

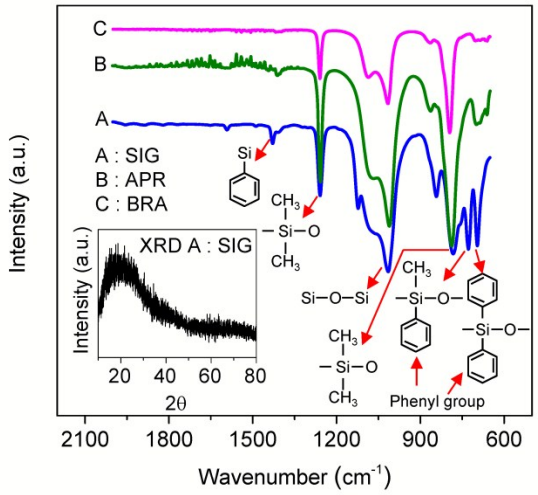

Fig. 1 FTIR spectra of silicone oil precursors from three different suppliers in the market and XRD pattern of as-annealed SIG sample (inset).

Raman spectroscopy was used to reveal the vibrational modes of the SiOC material (Fig. 2a). The Raman spectra of a Si/C composite (Fig. 2b) and pristine Si microparticles (Fig. 2c) are provided for comparison. The typical peaks at 508 and 933 cm^{-1} (Fig. 2b and Fig. 2c) represent the first and second Si-Si vibrational modes, respectively. In contrast, these intense bands were not observed in the SiOC sample due to the absence of Si-Si bonding in the as-prepared sample. This finding is consistent with previous data obtained by FTIR and XRD analysis. The presence of a free-carbon phase in the SiOC samples was confirmed by two distinct peaks at 1322 and 1596 cm^{-1}, attributed to the D and G-band, respectively. The small broad peaks in the wavelength range of 2700-3000 cm^{-1} were attributed to the 2D and D+G band, corresponding to sp^2 carbon and a mixture of two phonons with different momentums, respectively.[32-34]

We further carried out TEM element mapping, as displayed in Fig. 2d-g. The maps show a fair distribution of Si, O and C. The EDX analysis results in Fig. 2h confirm that the SiOC sample consisted of only three elements, highlighting the purity of the as-prepared samples. The chemical bonding of the SiOC sample was further elaborated by FTIR and XPS analysis (Fig. S3†). The Si-O-C bonding in SiOC was confirmed by a broad peak shown at 968 cm^{-1} in FTIR spectrum (Fig. S3a†).[35] The Si_{2p} peaks (Fig. S3b†) at 101.8, 102.7 and 103.5 eV are attributed to SiO_2C_2, SiO_3C and SiO_4, respectively.[36] The O_{1s} spectra (Fig. 3c†) indicate two peaks at 532.7 eV and 533.6 eV, corresponding to O-Si and Si-O-Si bonding, respectively.[15, 35] The C_{1s} spectra (Fig. S3d†) present seven deconvoluted peaks at 283.5, 284.4, 285.7, 286.7, 288.4, 290.1 and 291.9 eV, which represent Si-C, C=C, C-C, epoxy, C-O, C=O, and O-C=O bonding, respectively.[32, 37]

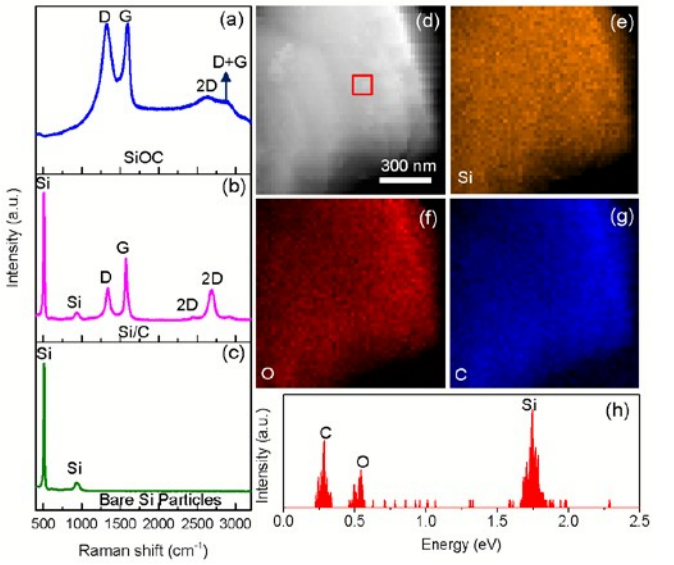

Fig. 2 Raman spectra of (a) SiOC, (b) Si/C composite, and (c) pristine Si microparticles. (d) High-resolution transmission electron microscopy (HRTEM) image and (e-g) elemental maps for Si, O, and C. (f) A representative EDX analysis of the area indicated in (d).

The electrochemical performance of SiOC was demonstrated by comparing the SiOC anode material with the conventional Si/C composite synthesized from ball-milled Si and MCMB powder. For direct comparison, a sample with Si/C composition ratio (6:4 wt%) similar to that of SiOC, as determined by XRF analysis (Table S1†), was prepared. The performance of SiOC and Si/C was then analysed under identical testing parameters. Fig. 3a shows the cycle capability of a Si/C composite and SiOC anode at a current density of 200 mAg^{-1} and cut-off voltage of 0.001 V–3.0 V. Although the initial capacity of the Si/C composite (1796 $mAhg^{-1}$) was higher than that of SiOC (676 $mAhg^{-1}$), the capacity of the Si/C composite rapidly decreased with cycling. The discharge capacity of the Si/C composite and SiOC anode material after 250 cycles was 222 and 804 $mAhg^{-1}$, respectively. The overall Coulombic efficiency (CE) of SiOC (99.8 %) was higher than that of the Si/C composite (98 %). A higher CE represents lower irreversible capacity loss and an enhancement of interface kinetics.[38] The SiOC anode also demonstrated a stable rate capability performance, as shown in Fig. 3b. The discharge capacity of SiOC at a current density of 100 mAg^{-1} was 852 $mAhg^{-1}$. When

the current density was increased to 6400 mAg^{-1}, the reversible capacity of SiOC was maintained at 772 $mAhg^{-1}$. We further examined the cycle performance of SiOC at various current densities of 50 mAg^{-1}, 200 mAg^{-1} and 1000 mAg^{-1} up to 80 cycles (Fig. S4†). At a low current density (50 mAg^{-1}), the discharge capacity of SiOC at the first cycle was 753 $mAhg^{-1}$. After 80 cycles, the capacity exceeded 900 $mAhg^{-1}$ and remained at 520 $mAhg^{-1}$ even under a high current density (1000 mAg^{-1}). No capacity fading was observed at the current densities considered in the study.

The superior cyclability, CE and rate capability performance might be attributed to the presence of an embedded free-carbon phase within the SiOC matrix. The disordered carbon structure provided a 3D curved network of sp^2 carbons, thereby resulting in a smaller Li-Li distance and a low barrier for Li^+ diffusion.[39] Our calculated lithium ion diffusion coefficient within SiOC was 5×10^{-6} cm^2 s^{-1} (Fig. S5†). This value is one to two orders of magnitude higher than the best reported lithium ion diffusion coefficient within SiOC, which was obtained from a polyramic RD-684a precursor.[22]

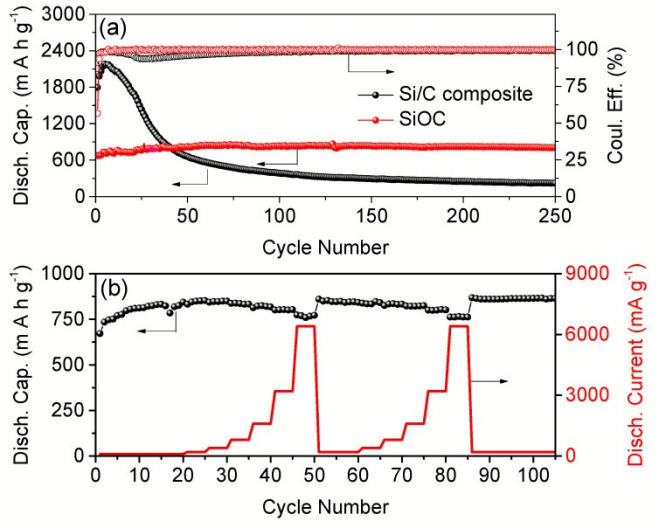

Fig. 3 (a) Cycle life performance of Si/C composite and SiOC at a current density of 200 mAg^{-1} (b) Cycle life performance of SiOC at varied discharging current densities (100–6400 mAg^{-1}). A cut-off voltage of 0.001–3.0 V was employed for both cycle and rate capability tests.

Ex-situ XRD investigations of the disassembled anodes at different applied voltages were executed in order to understand the mechanism of Li storage in SiOC materials (Fig. 4a). Prior to disassembling, the anodes were first discharged starting from 3.0, 0.75, 0.07 and 0.001 V, which are respectively represented by points A, B, C and D. Subsequently, the anodes were charged to 0.4, 1.0, 2.0 and 3.0 V, respectively assigned as points E, F, G and H. Fig. 4b shows the XRD spectra for Si/C composite anodes. At points A and B, we observed an intense peak at 26.4°, representing carbon (MCMB), and three other peaks at 28.5°, 47.4° and 56.2°, indicating crystalline Si. At a deeper lithiation state (point C), these three major peaks were slightly reduced, initiating an amorphous transformation of the Si crystal structure. After full lithiation at point D, the peaks of crystalline Si were greatly diminished due to the formation of $Li_{15}Si_4$.[40, 41] During delithiation, the Si/C composite was again transformed to the amorphous phase (point E), as indicated by the significant reduction in the intensity of the peak at 28.5° and the disappearance of the peaks at 47.4° and 56.2°. The XRD profiles at points F, G and H showed no crystalline Si peaks, indicating that the Si/C composite was again completely transformed into an amorphous phase. In contrast, the SiOC anode experienced no phase transformation at each lithiation/delithiation step, as shown in Fig. 4c. SiOC underwent a single-phase reaction throughout the lithiation and delithiation processes, thereby remaining amorphous.

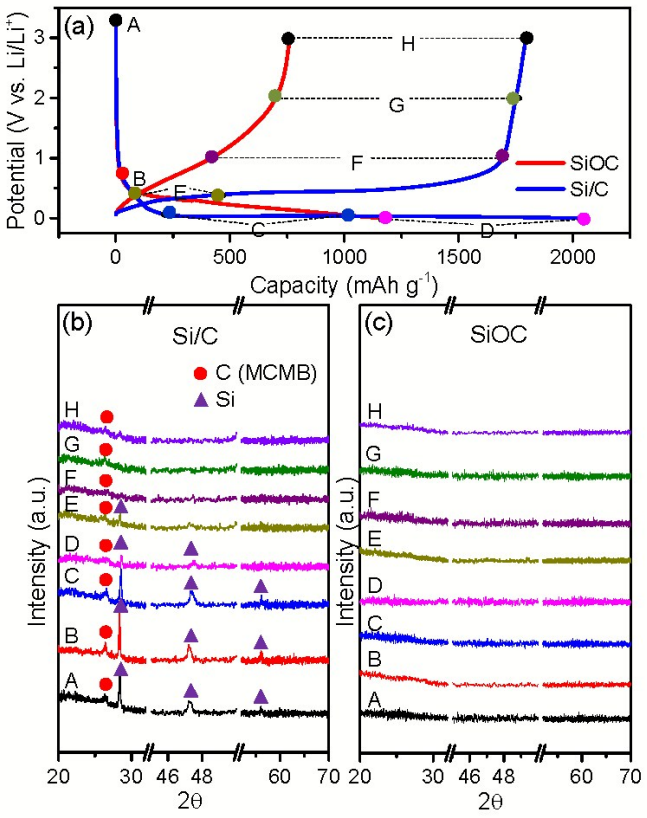

Fig. 4 (a) Voltage profiles of SiOC and Si/C composite materials with the respective measurements points (A-H) for XRD analysis. The XRD patterns of (b) Si/C composite material and (c) SiOC, according to the voltage points shown in (a). Notes: Breaks were given in the range of 32°-45° and 50°-52° in order to hide the intense peaks of Cu substrates.

Differences in the reaction mechanism of both materials were detected from CV profiles (Fig. S6†). The anodic and cathodic peaks in the CV curve of pure Si were correlated to the alloying and de-alloying mechanism.[42] The CV profile of the Si/C composite was similar to that of pristine Si, indicating that even if Si in the Si/C composite was mixed with carbonaceous material, the reaction mechanism would be based on alloying and de-alloying. In contrast, no anodic and cathodic peaks were observed in the CV profile of SiOC, pronouncing non-alloying/de-alloying reaction. Fukui and colleagues revealed that the lithium storage mechanism in SiOC materials is similar to that of in hard carbon anode, following intercalation/deintercalation processes.[43, 44] Using ^7Li NMR resonance, they

found that the lithium intercalation sites took place in micropores (< 2 nm) and in the interstitial spaces and/or edge of graphene layers.

The Li^+ storage mechanism of the SiOC electrode affects the dimensional stability of the electrode, determining the electrochemical performance during cycling. The major disadvantage of anode materials that form Li alloys, such as Si-based materials, is that the formation involves breaking bonds between host atoms, leading to severe volume changes, and ultimately, pulverization.[45] To investigate the volume change during the cycle, we opened the post-cycled cells and observed the thickness of the electrodes by SEM, as shown in Fig. 5. The initial thickness of the Si/C composite (Fig. 5a) and SiOC material (Fig. 5e) before the cycle were comparable, 10.2 µm and 10.4 µm, respectively. After the first lithiation, the thickness of the Si/C composite (Fig. 5b) and SiOC electrodes (Fig. 5f) increased by 107.5% and 6.4%, respectively. When delithiation was performed, the thickness of the Si/C composite (Fig. 5c) and SiOC electrodes (Fig. 5g) compressed to 7% and 4.8% higher than its initial thickness, respectively. After a prolonged cycle (delithiation at 50 cycles), the thickness of the Si/C composite (Fig. 5d) and SiOC electrodes (Fig. 5h) increased by 302.7% and 35.6%, respectively. This finding supports our hypothesis that the lithiation/delithiation mechanism in the SiOC material is not based on alloying/de-alloying; hence, the volume change during cycling can be minimized. Liao *et al*. suggested that a denser structure might be formed during the insertion of Li^+ ions into the matrix of a SiOC anode.[46]

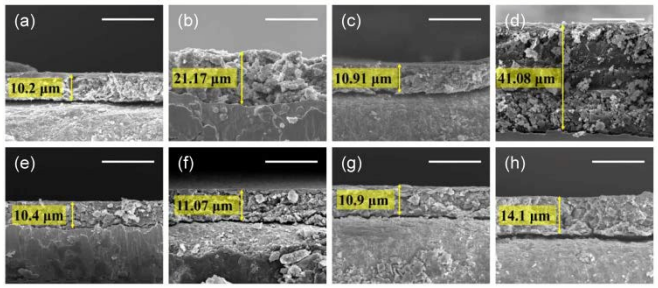

Fig. 5 Cross-sectional SEM images of Si/C composite electrodes (a) before cycling, (b) after 1st lithiation, (c) after 1st delithiation, and (d) after 50 cycles. These results are compared with cross-sectional SEM images of a SiOC electrode (e) before cycling, (f) after 1st lithiation, (g) after 1st delithiation, and (h) after 50 cycles. Note : the bar scale in each figure denotes 20 µm.

It is interesting to compare our SiOC material with other SiOC anodes derived from other precursors available in the literature, as shown in Fig 6. Fig. 6a compares our SiOC to that reported by Pradeep *et al*.[19] at a similar charge—discharge current density. Our SiOC exhibited higher discharge capacity over any range of current density. Fig. 6b compares our study with that of Ahn and coworker;[17] we applied a constant charge current density of 100 mAg^{-1} and varied the discharge current density from 100 to 6400 mAg^{-1}. The discharge capacity of SiOC at a current density of 100 mAg^{-1} was 852 $mAhg^{-1}$. When the current density was increased 64 fold, 90% of the initial discharge capacity (772 $mAhg^{-1}$) could be maintained. Our SiOC material clearly outperforms the SiOC synthesized from a mixture of 1,3,5,7-tetramethyl- 1,3,5,7-tetravinylcyclotetrasiloxane and dicumyl peroxide.[17] Fig. 6c shows the galvanostatic cycle performance of our SiOC material at different current densities in comparison to the SiOC materials derived from Polyramics RD-684.[18] Current densities of 37, 74, 372 and 37 mAg^{-1} were tested for 10, 20, 30 and 10 cycles respectively. The highest discharge capacity of our SiOC was ~900 $mAhg^{-1}$ at 37 mAg^{-1}. Our result surpassed the discharge capacity of SiOC studied by Riedel's group at all current densities. A detailed comparison of electrochemical performance between our SiOC derived from silicone oil and other precursors is given in Table S2†.

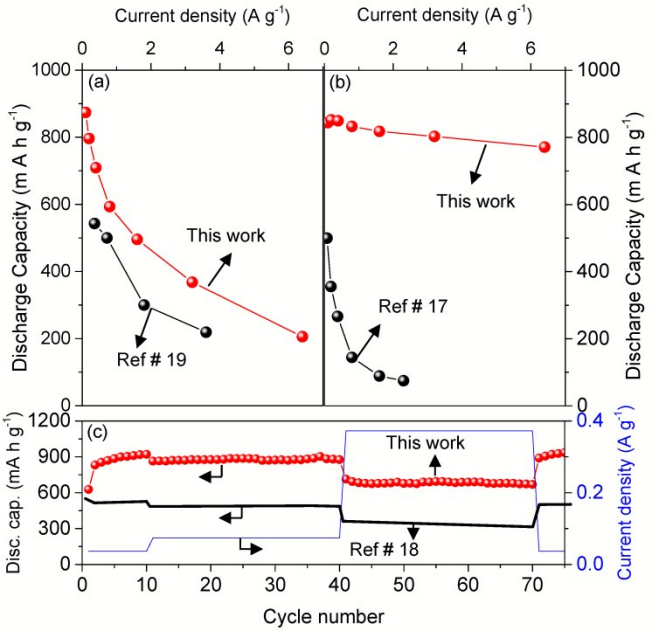

Fig. 6 Comparison of electrochemical performance of SiOC derived from phenyl-rich silicone oil and SiOC synthesized from different precursors available in the literature. (a) Rate capability of our SiOC vs. that in Pradeep and co-workers' study (Ref#19), (b) rate capability of our SiOC vs. that in Ahn et al.'s study (Ref#17), and (c) rate capability with prolonged cycles of our SiOC vs. that in Kaspar et al.s' study (estimated redrawing from Ref#18). For all comparisons, we followed identical electrochemical testing procedures.

Conclusions

In summary, we synthesized a SiOC anode from a silicone oil precursor via a simple and scalable pyrolytic method. In particular, we discovered that silicone oil with a phenyl-rich group yielded SiOC materials with an embedded free-carbon phase. The as-prepared SiOC anode exhibited excellent long-cycle performance, high Coulombic efficiency and high rate capability due to its extremely low dimensional change over cycles and relatively fast Li^+ mobility within the SiOC matrix. In addition, our SiOC material underwent a non-alloying reaction mechanism, unlike conventional Si-based materials, which prevented the structural breakdown of the host atoms involved in bonding. The present study not only indicates the promising commercialization of a SiOC anode in LIBs, but also

opens the possibility for use in other energy storage devices such as hybrid supercapacitors, which can provide high power, high energy and long cycle life.

Acknowledgments

M. Halim and C. Hudaya contributed equally to this work. This work was supported by Korea Institute of Science and Technology (KIST) institutional program and by research grants funded by the National Research Foundation under the Ministry of Science, ICT & Future Planning, Korea (NRF-2012M1A2A2671792). The authors also thank Mr. Joo Man Woo and Mr. Un Seok Kim for technical discussion during preparation of this study.

References

1. B. Scrosati, *Electrochim. Acta*, 2000, **45**, 2461-2466.
2. M. Endo, C. Kim, K. Nishimura, T. Fujino and K. Miyashita, *Carbon*, 2000, **38**, 183-197.
3. J. M. Tarascon and M. Armand, *Nature*, 2001, **414**, 359-367.
4. M. Armand and J. M. Tarascon, *Nature*, 2008, **451**, 652-657.
5. J. B. Goodenough and K. S. Park, *J. Am. Chem. Soc.*, 2013, **135**, 1167-1176.
6. J. J. Chen, *Materials*, 2013, **6**, 156-183.
7. S. Park, T. Kim and S. M. Oh, *Electrochem. Solid St.*, 2007, **10**, A142-A145.
8. D. Mazouzi, B. Lestriez, L. Roue and D. Guyomard, *Electrochem. Solid St.*, 2009, **12**, A215-A218.
9. U. Kasavajjula, C. S. Wang and A. J. Appleby, *J. Power Sources*, 2007, **163**, 1003-1039.
10. M. N. Obrovac, L. Christensen, D. B. Le and J. R. Dahnb, *J. Electrochem. Soc.*, 2007, **154**, A849-A855.
11. J. S. Kim, M. Halim, D. Byun and J. K. Lee, *Solid State Ionics*, 2014, **260**, 36-42.
12. A. M. Wilson, J. N. Reimers, E. W. Fuller and J. R. Dahn, *Solid State Ionics*, 1994, **74**, 249-254.
13. J. Kaspar, M. Graczyk-Zajac and R. Riedel, *J. Power Sources*, 2013, **244**, 450-455.
14. D. Larcher, C. Mudalige, A. E. George, V. Porter, M. Gharghouri and J. R. Dahn, *Solid State Ionics*, 1999, **122**, 71-83.
15. L. J. Ning, Y. P. Wu, L. Z. Wang, S. B. Fang and R. Holze, *J. Solid State Electr.*, 2005, **9**, 520-523.
16. F. Ji, Y. L. Li, J. M. Feng, D. Su, Y. Y. Wen, Y. Feng and F. Hou, *J. Mater. Chem.*, 2009, **19**, 9063-9067.
17. D. Ahn and R. Raj, *J. Power Sources*, 2011, **196**, 2179-2186.
18. J. Kaspar, M. Graczyk-Zajac and R. Riedel, *Solid State Ionics*, 2012, **225**, 527-531.
19. V. S. Pradeep, D. G. Ayana, M. Graczyk-Zajac, G. D. Soraru and R. Riedel, *Electrochim. Acta*, 2015, **157**, 41-45.
20. T. Momma, S. Aoki, H. Nara, T. Yokoshima and T. Osaka, *Electrochem. Commun.*, 2011, **13**, 969-972.
21. M. Graczyk-Zajac, L. Toma, C. Fasel and R. Riedel, *Solid State Ionics*, 2012, **225**, 522-526.
22. J. Kaspar, M. Graczyk-Zajac and R. Riedel, *Electrochim. Acta*, 2014, **115**, 665-670.
23. P. Dibandjo, M. Graczyk-Zajac, R. Riedel, V. S. Pradeep and G. D. Soraru, *J. Eur. Ceram. Soc.*, 2012, **32**, 2495-2503.
24. F. Zhou, Y. M. Liang and W. M. Liu, *Chem. Soc. Rev.*, 2009, **38**, 2590-2599.
25. P. J. Launer, in *Silicone Compounds Register and Review*, ed. B. Arkles, Petrarch Systems, 1987, pp. 100-103.
26. G. Mera, A. Navrotsky, S. Sen, H. J. Kleebe and R. Riedel, *J. Mater. Chem. A*, 2013, **1**, 3826-3836.
27. T. H. Elmer and H. E. Meissner, *J. Am. Ceram. Soc.*, 1976, **59**, 206-209.
28. H. Zhang and C. G. Pantano, *J. Am. Ceram. Soc.*, 1990, **73**, 958-963.
29. M. Graczyk-Zajac, G. Mera, J. Kaspar and R. Riedel, *J. Eur. Ceram. Soc.*, 2010, **30**, 3235-3243.
30. G. M. Renlund, S. Prochazka and R. H. Doremus, *J. Mater. Res.*, 1991, **6**, 2723-2734.
31. G. D. Soraru, G. Dandrea, R. Campostrini, F. Babonneau and G. Mariotto, *J. Am. Ceram. Soc.*, 1995, **78**, 379-387.
32. X. Diez-Betriu, S. Alvarez-Garcia, C. Botas, P. Alvarez, J. Sanchez-Marcos, C. Prieto, R. Menendez and A. de Andres, *J. Mater. Chem. C*, 2013, **1**, 6905-6912.
33. R. S. Diggikar, D. J. Late and B. B. Kale, *Rsc Adv.*, 2014, **4**, 22551-22560.
34. D. C. Elias, R. R. Nair, T. M. G. Mohiuddin, S. V. Morozov, P. Blake, M. P. Halsall, A. C. Ferrari, D. W. Boukhvalov, M. I. Katsnelson, A. K. Geim and K. S. Novoselov, *Science*, 2009, **323**, 610-613.
35. Q. Xia, B. Wang, Y. P. Wu, H. J. Luo, S. Y. Zhao and T. van Ree, *J. Power Sources*, 2008, **180**, 602-606.
36. R. J. P. Corriu, D. Leclercq, P. H. Mutin and A. Vioux, *J. Sol-Gel Sci. Techn.*, 1997, **8**, 327-330.
37. E. B. Nursanto, A. Nugroho, S. A. Hong, S. J. Kim, K. Y. Chung and J. Kim, *Green. Chem.*, 2011, **13**, 2714-2718.
38. C. Hudaya, M. Halim, J. Proll, H. Besser, W. Choi, W. Pfleging, H. J. Seifert and J. K. Lee, *J. Power Sources*, 2015, **298**, 1-7.
39. D. Odkhuu, D. H. Jung, H. Lee, S. S. Han, S. H. Choi, R. S. Ruoff and N. Park, *Carbon*, 2014, **66**, 39-47.
40. M. N. Obrovac and L. Christensen, *Electrochem. Solid St.*, 2004, **7**, A93-A96.
41. W. J. Zhang, *J. Power Sources*, 2011, **196**, 877-885.
42. M. Green, E. Fielder, B. Scrosati, M. Wachtler and J. Serra Moreno, *Electrochem. Solid St.*, 2003, **6**, A75-A79.
43. H. Fukui, H. Ohsuka, T. Hino and K. Kanamura, *Acs Appl. Mater. Inter.*, 2010, **2**, 998-1008.
44. H. Fukui, H. Ohsuka, T. Hino and K. Kanamura, *J. Electrochem. Soc.*, 2013, **160**, A1276-A1281.
45. M. T. McDowell, S. W. Lee, W. D. Nix and Y. Cui, *Adv. Mater.*, 2013, **25**, 4966-4984.
46. N. B. Liao, B. R. Zheng, H. M. Zhou and W. Xue, *J. Mater. Chem. A*, 2015, **3**, 5067-5071.